FLOMEKO 2003
11th IMEKO TC9 Conference on Flow Measurement
Groningen, NETHERLANDS, 12 - 14 May 2003

FLOW BEHAVIOR IN SONIC MICRO-NOZZLES

E. von Lavante, University of Essen, Essen, Germany
R. Kramer, B. Mickan, PTB, Braunschweig, Germany

Abstract
Detailed investigation of flow fields associated with sonic Venturi nozzles with extremely small Reynolds numbers used for flow metering was carried out. The range of Reynolds numbers considered in this work extended from Re = 323 to Re = 452. In the experimental part, global parameters such as discharge coefficient C_d were investigated independently for two different diameters, d = 25 μm and d = 35 μm. Both discovered flow phenomena that were not explainable using simple linear theories. Therefore, in the numerical part of the present investigation, the corresponding flow fields were simulated using compressible viscous flow solvers ACHIEVE and Fluent. The qualitative agreement of the numerical and experimental results was satisfactory; the comparison enabled the authors to explain most of the physical phenomena observed.

Introduction
The use of sonic nozzles in metrology is regulated by the still valid standard ISO 9300 [1]. Accordingly, the validity range of the corresponding measurement is limited to Reynolds numbers between 10^5 and 10^7. Many times, however, it is desirable to use nozzles at much smaller Reynolds numbers, either for applications with very small volumetric flows resulting in small throat diameters, or for metering gases at very small pressures. In these cases, several investigators [3] [4] [5] [9] have discovered flow effects that were inconsistant with the simple quasi-one-dimensional theory. These included variation of the discharge coefficient C_d as a function of the nozzle back pressure, not explainable by the theory offered in ISO 9300 [1], occurance of instabilities and pressure waves traveling upstream all the way through the throat and thus unchoking the nozzle for a very brief period of time, and the so called premature unchoking. After calibration, however, the corresponding nozzles still offer the same very reliable means of gas metering. Critical nozzles are already in use in legal metrology for flow rates down to less than few liters per hour in, for instance, Q_{min} -verification of diaphragm household gasmeters. Besides, there is a significant demand for reliable and stable measuring techniques of small flow rates in the fields of medical, chemical or enviromental applications. To realize such small flow rates, the required nozzles must have diameters much less than 1 mm, typically in the order of several μm, with the corresponding Reynolds numbers orders of magnitude below the minimum given by the ISO standard. These extremely small sonic Venturi nozzles still possess the same basic advantages of their larger counterparts. They represent a robust, consistent, simple and reliable means of metering gases and, after proper calibration, are potentially highly accurate.

The good experience made by the present authors as well as many other investigators with small sonic nozzles employed in metrology justified further study of the corresponding flow fields. It was hoped to gain more detailed knowledge of the behavior of these nozzles when applied to meter small mass flows. This, in turn, should make an explanation of most of the unusual effects occuring in these configurations possible.

With this motivation in mind, the present authors undertook an experimental and numerical investigation of air flow in sonic micro-nozzles, characterized by extremely small Reynolds numbers given by nozzle diameters in the range of μm. The shape as well as dimensions of one of the nozzles is given in Figure 1. The close cooperation between the experimental and numerical parts of this study was of advantage when explaining some of the physical phenomena occuring in these nozzles.

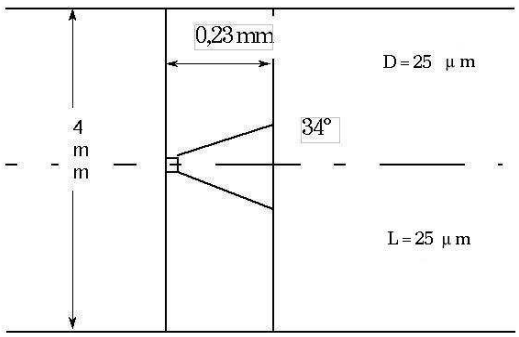

Figure 1: Typical nozzle shape and dimensions for a nozzle characterized by Re = 323.

Physics of the case studied
The micro-nozzle investigated in the present work consisted of a cylindrical section of either $D = 25$ μm or $D = 35$ μm throat diameter and a conical section having an opening angle of $\phi = 34^o$. The remaining dimensions are given in Figure 1. The corresponding Reynolds numbers were $Re = 323$ and $Re = 452$, respectively. The nozzles were manufactured mechanically using punching, resulting in a surprisingly regular shape. A photograph of the nozzle, as seen from the conical end, can be viewed in the left part of Figure 2. The same nozzle is displayed in the right part of Figure 2 as seen from the cylindrical end. It is interesting to note that laser drilling produced much worse shapes.

The gas metered by the nozzles was air at atmospheric conditions. The inflow pressure was approximately $p_{in} =$ 1.01325 bar (101325 Pa) and the temperature $T_{in} = 300$ K. Since the inflow area was much larger than the throat

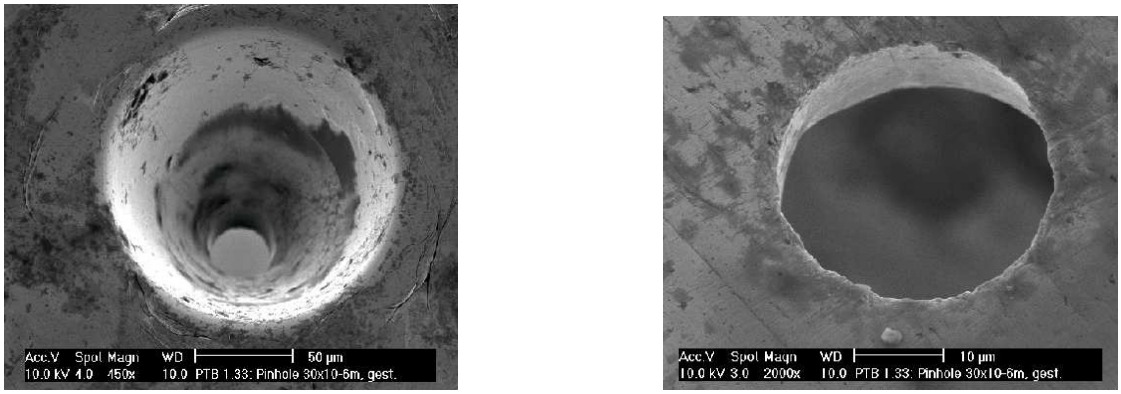

Figure 2: Photograph of the nozzle taken from the conical end (left) and the cylindrical end (right).

area, it was save to assume that $p_{in} = P_0$. The exit pressure was varied setting it to $p_{out}/P_0 = 0.6, 0.5, 0.35, 0.2$ and 0.1. The primary direction of air flow through the nozzle was similar to its ISO9300 counterpart, with the conical diffusor oriented toward the exit. In Figure 1, the gas would be flowing from left to right, resulting in an arrangement called "normal" or "forward". The nozzle was also tested with the conical part oriented toward the inlet, with flow going from right to left in Figure 1. This setup was called "reverse" or "backward".

Numerical Algorithms

Due to the different requirements imposed on the solver depending on the flow direction through the nozzle, two numerical methods were used. In the case of "forward" flow, the solver ACHIEVE was used due to its low numerical dissipation, necessary for the correct simulation of the free jet. The "backward" flow nozzle required the more disipative but robust commercial solver Fluent, presently used in its version 6.x. They will be described separately below.

The numerical method employed in the present flow simulations is part of a flow simulation system developed at the Institute of Turbomachinery at the University of Essen, called "ACHIEVE". It consists of an upwind solver of the Navier-Stokes equations, using finite volume discretization. The governing equations to be solved in the present simulations are the axisymmetric compressible Navier-Stokes equations. The governing equations are given in more detail by, for example, Steger [7] or von Lavante et. al. [6]. The features of the two solvers are compared in Table 1.

Table 1: Solver features used in the present numerical simulations.

ACHIEVE	Fluent
Roe's flux difference splitting in finite volume form	coupled implicit solver (Roe FDS, finite volume)
two-stage modified Runge-Kutta time stepping	second order implicit method in pseudo-time
k-ω-turbulence model	k-ϵ-turbulence model
compressible flow	compressible flow
ideal gas law	ideal gas law
blockstructured grid	hybrid grid (structured in b.l., unstructed in far-field)
multiblock structure; fully parallelized	multiblock structure; moderately parallelized

The computational grid generation was accomplished using the GRIDGEN program, since it allowed the combination of blocks of structured grids to be generated while being relatively easy to use (for more details, see the next section). Nonreflecting boundary conditions had to be used throughout the computational domain. The computations were carried out on a cluster of PC-type workstations using the Linux OS. The cluster is connected by a high performance network, making moderately parallelized computations possible.

Computational grid

The computational grid used in the present simulations can be seen in Figure 3, with the different blocks clearly marked.

The total grid consisted of $20 \cdot 10^3$ number of points. Particular attention was paid to sufficient resolution in areas of high flow variable gradients, such as bounary layers or shear layers. The problem was parallelized such that each block of grids was associated with one CPU.

Experimental setup at PTB

In order to investigate the behavior of nozzles, stable inflow conditions are very important. Such conditions can be achieved if atmospheric air is drawn through the nozzles. A schematic picture of the present experimental setup is presented in figure 4. By using high resolution digital barometer as a pressure sensor, very sensitive measurement of intake pressure was possible. During the investigations, the flow rate given by the nozzle was measured by a mass

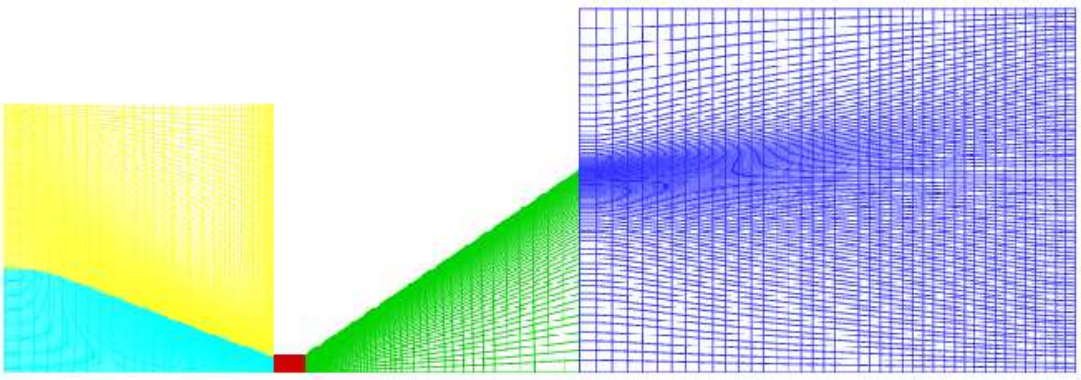

Figure 3: View of the computational grid.

flow element, installed directly in front of the nozzle. The element used displayed good repeatability and reproducibility. The repeatability was 0.01 ml/min. Downstream of the nozzle, a control valve and a vacuum pump were installed. The control valve was designed for a very wide flow range. It allowed the stabilization of the pressure at the nozzle outflow resulting in fluctuations smaller than 1 mbar. During the investigation, the observed changes of atmospheric pressure were smaller than 0.05 mbar; hence no corrections of the input pressure were necessary. The flow rate determined by the nozzles was measured in both installation directions 5 times, beginning at the lowest output pressure. For the same pressure ratios, no differences in the readouts were observed, meaning that no shift of the MFE occurred.

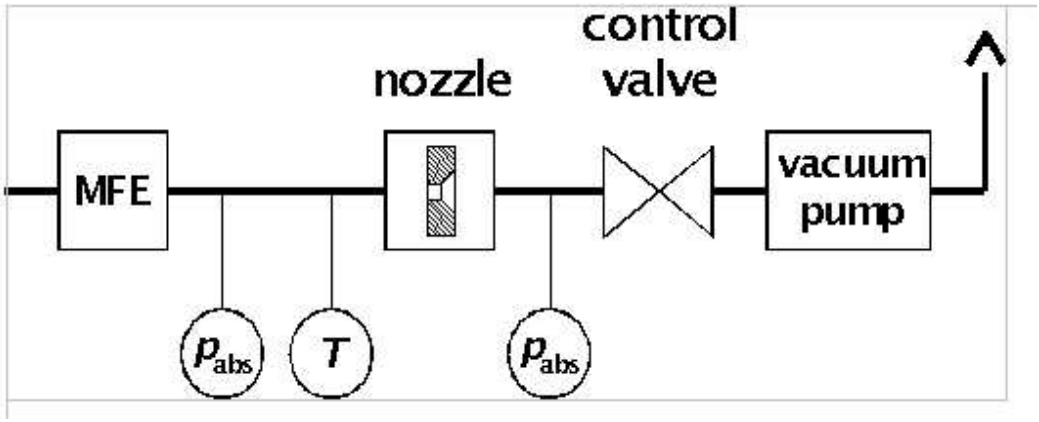

Figure 4: Setup used for the investigation of the nozzles.

In the present experimental work concerning the flow behavior in the micro nozzles, the MFE was used as a flow rate indicator. In order to calibrate the micro nozzles, the PTB uses a piston prover shown in Fig. 5. A new type of piston prover using an actively moved piston was developed for particularly low flow rates. The system allowed the calibration transfer standards like MFE or LFE as well as micro nozzles with an uncertainty of $U = 0.05$ % ($k = 2$).

In order to match the flow rate generated by the piston prover to the flow rate determined by a nozzle, very stable and sensitive adjustment of the revolution speed of the driving motor was necessary. Adequate properties were achieved by using a stepping motor system. The stepper motor allowed 10 000 steps per rotation. The speed of revolution was changeable by 1 step/rotation.

The flow indication instrument at the intake of the facility was used only for the above mentioned matching of the flow rates. During the calibration, the input valve was closed. If the flow rate of the nozzle and the piston proover were not exactly equal, a slow change of input pressure of the nozzle could be observed. A correction algorithm, taking volume and pressure changes into consideration, allowed achieving the claimed uncertainties even if small pressure changes occured during the calibration. First results of the calibration showed a reproducibility of micro nozzles in the range of $U \leq 0.2$ % (k=2), but further investigations will be necessary to study the influence of parameters such as input pressure and temperature. In order to avoid dust-induced effects, a micro filter should be installed in front of the nozzles during the measurement.

Results

Experimental results

Several micro-nozzles were investigated at the PTB; here, the results will be summarized and discussed concentrating on two particular nozzles having throat diameters of $D = 25$ μm and $D = 35$ μm. The shape was the

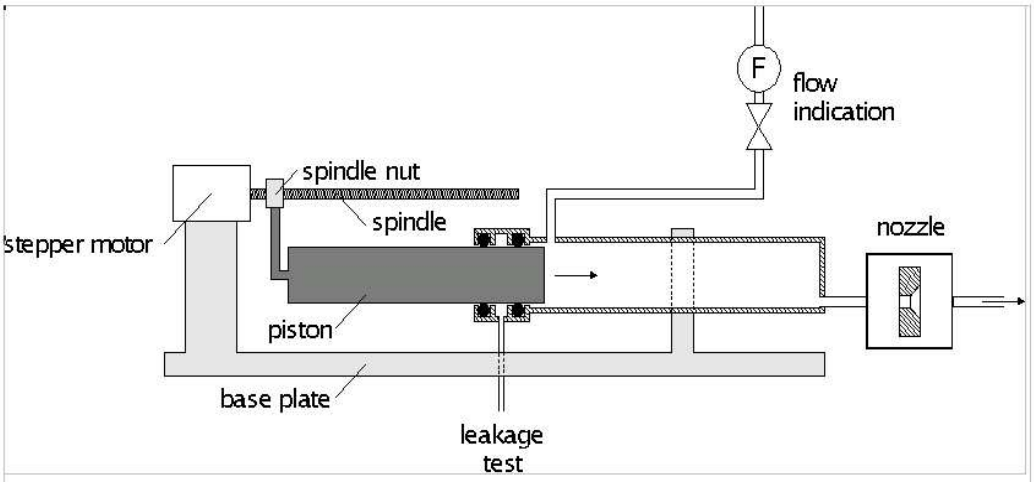

Figure 5: Schematic picture of the piston prover.

same as shown in Figures 1, 2 and 3. The coefficient C_D, as defined in the ISO 9300, is summerized in table 2 for the D = μm nozzle.

Table 2: Summary of flow rate coefficient C_D, $D = 25\mu m$.

P_{out}/P_0	0.6	0.5	0.35	0.2	0.1
Experim., forward	0.642	0.658	0.664	0.664	0.664
Experim., backwrd.	—	0.66	0.675	0.679	0.68
Num., forward	0.67	0.704	0.727	0.728	0.729
Num., backward	0.773	0.814	0.841	0.866	0.883

In the above table 2, the reference mass flow of the equivalent one-dimensional nozzle was $\dot{m}_{1-D} = 1.161 \cdot 10^{-7}$. The experimental data are best viewed in Figure 6 for $D = 35$ μm and in Figure 7 for $D = 25$ μm. Due to the similarity of both figures, only the results in Figure 7 will be discussed.

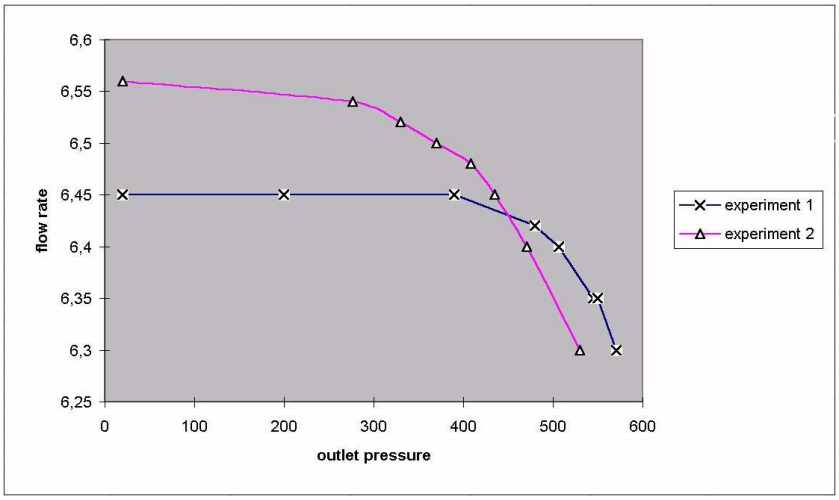

Figure 6: Mass flow rate through a micro-nozzle with a diameter of $D = 35$ μm and $Re = 452$.

The forward oriented nozzle behaved es expected. Starting from the highest pressure ratio of $P_{out}/P_0 = 0.6$, at which, obviously, the nozzle was not chocked, decreasing P_{out}/P_0 yielded an increase in mass flow until the nozzle chocked at approximately $P_{out}/P_0 = 0.35$. This critical pressure ratio is much smaller than the theoretical value of 0.528..., indicating that this is a case of premature unchocking. Below $P_{out}/P_0 = 0.35$, however, the nozzle remains chocked and the mass flow is consequently constant.

In striking contrast, the backward oriented nozzle behaved as a regular cylindrical micro-nozzle, with mass flow slightly increasing even after reaching $M = 1.0$ in the throat. There is no evidence of the classical choked condition.

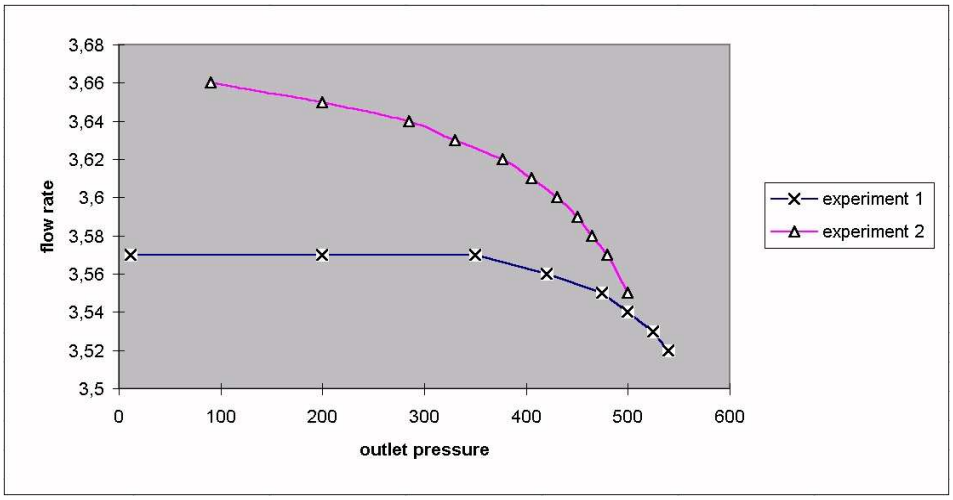

Figure 7: Mass flow rate through a micro-nozzle with a diameter of $D = 25$ μm and $Re = 323$.

In order to explain the above behavior, the $D = 25$ μm nozzle in Fig. 7 was subjected to numerical flow simulation. In the forward direction, the solver ACHIEVE was implemented. In this case, the correct simulation of the separation downstream of the cylindrical throat and the jet mixing outside of the nozzle required a code that displayed very low numerical dissipation. The resulting flow field can be viewed in Fig. 8 for the pressure ratio of $P_{out}/P_0 = 0.2$.

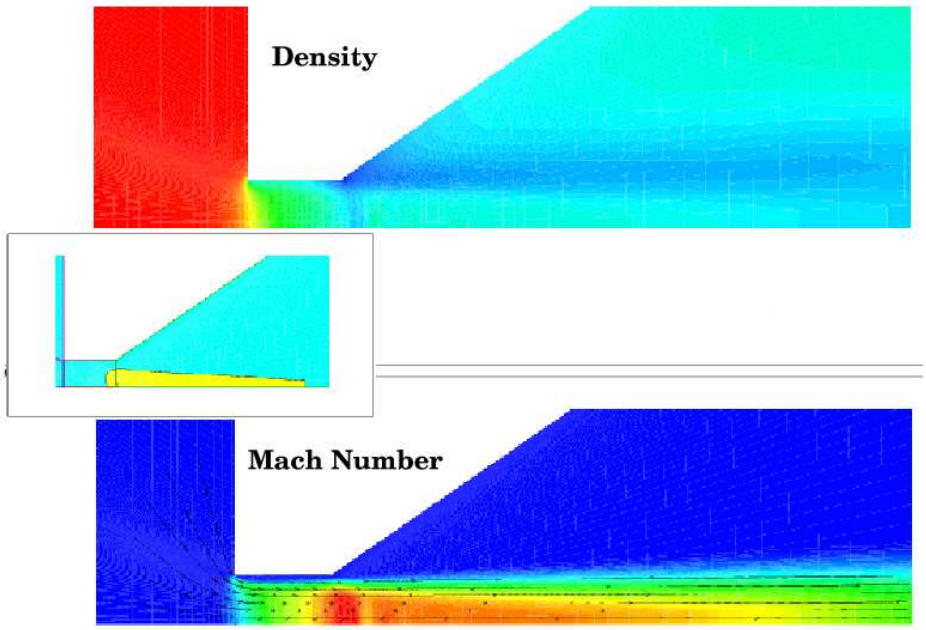

Figure 8: Flow field in micro-nozzle with a diameter of $D = 25$ μm and $Re = 323$, $P_{out}/P_0 = 0.2$.
Top: density contours;
Insert: extend of$M \geq 1$ (yellow);
Bottom: Mach number contours.

As the conical would-be diffusor has an opening angle of 34 degrees, the flow separates immediately after leaving the cylindrical part. The free jet then mixes with the surrounding fluid, causing recirculation at the conical wall. The highest Mach number of approximately 1.5 was reached after the flow expanded, forming subsequently a Mach disk that is clearly recognizable. Toward the nozzle exit, the jet dissipated, mixing with the surrounding quiescient air. The relatively coarse grid at this location resulted in somewhat higher rate of dissipation as expected.

At the lower pressure ratio of $P_{out}/P_0 = 0.1$, shown in Fig.9, the flow accelerates to even higher Mach numbers, exceeding $M = 2.0$. The flow becomes unstable, with pressure fluctuations within the free jet. There are several Mach disks visible downstream of the throat. However, more importantly, within the cylidrical part of the nozzle, the flow remains the same as compared to $P_{out}/P_0 = 0.2$. The boundary layer thickness is also very similar, resulting in approximately the same mass flow rate.

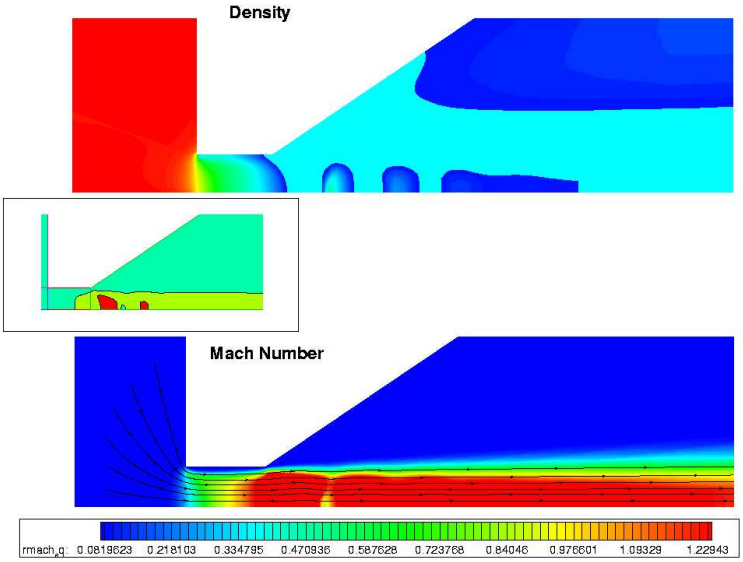

Figure 9: Flow field in micro-nozzle with a diameter of $D = 25$ μm and $Re = 323$, $P_{out}/P_0 = 0.1$.
Top: density contours;
Insert: extend of $M \geq 1$ (yellow), M 2 (red);
Bottom: Mach number contours.

Looking at the simulated flow field in the backward oriented nozzle in Figure 10, a totally different picture can be seen.

A relatively thick boundary layer developed along the conical wall that formed this time the inlet to the cylindrical part. Particularly in the later part of the nozzle, the shape of the bounary layer was a function of the incoming flow as well as velocity distribution in the throat. Consequently, the mass flow changed as a function of the pressure ratio even after the critical condition was reached.

Figure 11 shows the flow field just after $M = 1$ was reached downstream of the throat. In the insert, a simplified contours of the Mach number can be seen, with red marking areas of $M \geq 1.0$. Although the maximum Mach number is larger than in the case of $P_{out}/P_0 = 0.5$, the extent of the supersonic bubble is relatively small.

Finally, in Figure 12, the flow field for the case $P_{out}/P_0 = 0.1$ can be seen. The maximum Mach number is approximately 1.85. Noticeable is the reduction of the boundary layer thickness as well as the change of location of the zone of supersonic speed. Due to this continuous change of flow field in the throat, the mass flow could not remain constant and increased with decreasing pressure ratio, even after the nozzle reached supersonic Mach numbers.

Conclusions
The different behavior of the flow in the micro-nozzles under investigation can be traced back to the boundary layer effects. In the case of the forward flow nozzle, the air expanded outside of the cylindrical throat and maintained approximately the same location relative to the throat. After the chocked condition was reached, the mass flow remained essentially constant (see Table 2).

In the backward oriented nozzle, the changing boundary layer thickness and the shift in location of the $M = 1.0$ line resulted in a change of the mass flow even after the critical conditions were reached.

Future work will concentrate on the details of the corresponding flow fields, modification of the geometric parameters and, possibly, three-dimensional effects.

References

[1] International Standard ISO 9300, "Measurement of gas flow by means of critical flow Venturi nozzles", First Edition, Beuth, Berlin 1990.

[2] von Lavante, E. and Grönner, J., "Semiimplicit Schemes for Solving the Navier-Stokes Equations", 9th GAMM Conference, Lausanne, Notes on Numerical Fluid Mechanics, Vieweg, 1992.

[3] von Lavante, E., Nath, B. and Dietrich, H., "Effects of Instabilities on Flow Rates in Small Sonic Nozzles", Proceedings of the 9th Int. Conference on Flow Measurement FLOMEKO'98, Lund, 1998.

[4] Ishibashi, M., von Lavante, E. and Takamoto, M., "Quasi- Nonintrusive Measurement of Flow Velocity Field in a Critical Nozzle", Proceedings of ASME FEDSM'00, June 11-15, Boston, 2000.

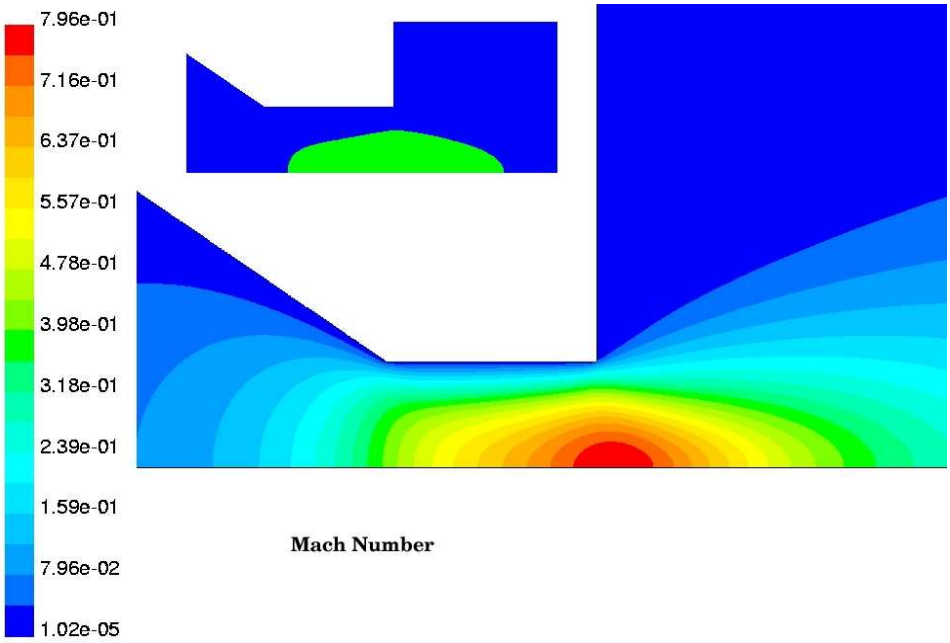

Figure 10: Flow field in backward micro-nozzle with a diameter of $D = 25$ μm, $P_{out}/P_0 = 0.5$, Mach contours.

[5] Wendt, G., Ph.D. Thesis, University of Essen, Germany, 2000.

[6] von Lavante, E., El-Milligui, A. and Warda, H., "Simulation of Unsteady Flows Using Personal Computers", The 3rd Int. Congress on Fluid Mechanics, Cairo, 1990.

[7] Steger, J. L., "Implicit, Finite-Difference Simulation of Flow about Arbitrary Geometries", AIAA Journal, Vol. 16, No. 7, 1978.

[8] von Lavante, E., El-Miligui, A., Cannizzaro, F. E., and Warda, H. A., "Simple Explicit Upwind Schemes for Solving Compressible Flows", Proceedings of the 8th GAMM Conference on Numerical Methods in Fluid Mechanics, Delft, 1990.

[9] Nakao, Shin-ichi, "Choking Phenomenon of Sonic Venturi Nozzles on Low Reynolds Numbers", Proceedings of the 9th Int. Conference on Flow Measurement FLOMEKO'98, Lund, 1998.

[10] Ishibashi, M. and Takamoto, M., "Very Accurate Analytical Calculation of the Discharge Coefficient of Critical Venturi Nozzles with Laminar Boundary Layer", Proceedings of the FLUCOME97, Hayama, Japan, Sept. 1997.

[11] von Lavante, E., Zachcial, A., Zeitz, D., Nath, B. and Dietrich, H., "Effects of Various Geometric Parameters on the Flow Behavior in Sonic Nozzles", Proceedings of the 10th Int. Conference on Flow Measurement FLOMEKO'2000, Salvador, 2000.

[12] von Lavante, E., Zachcial, A., Färber, J., Nath, B. and Dietrich, H., "Simulation of Unsteady Effects in Sonic Nozzles Used for Flow Metering", Proceedings of the 8th Int. Symposium on Computational Fluid Dynamics, Bremen, Sept. 1999.

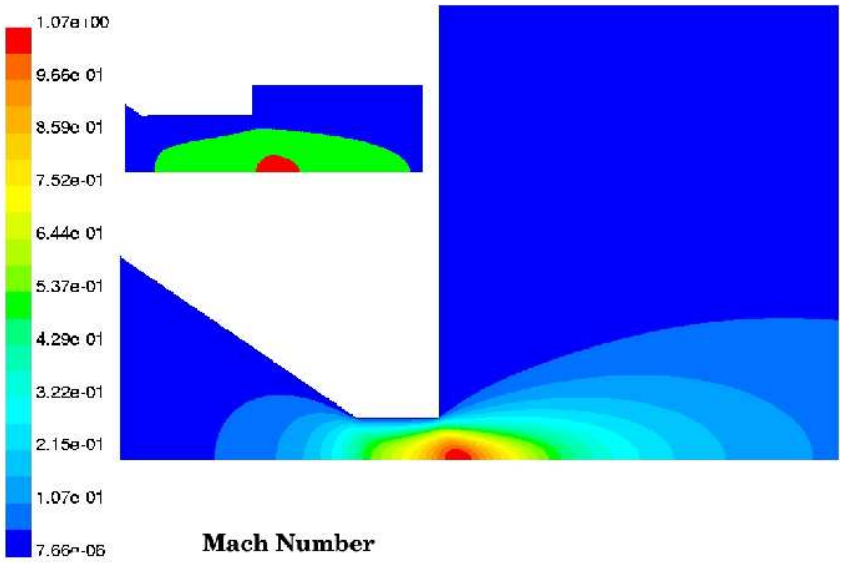

Figure 11: Flow field in backward micro-nozzle with a diameter of $D = 25$ μm, $P_{out}/P_0 = 0.35$, Mach contours.

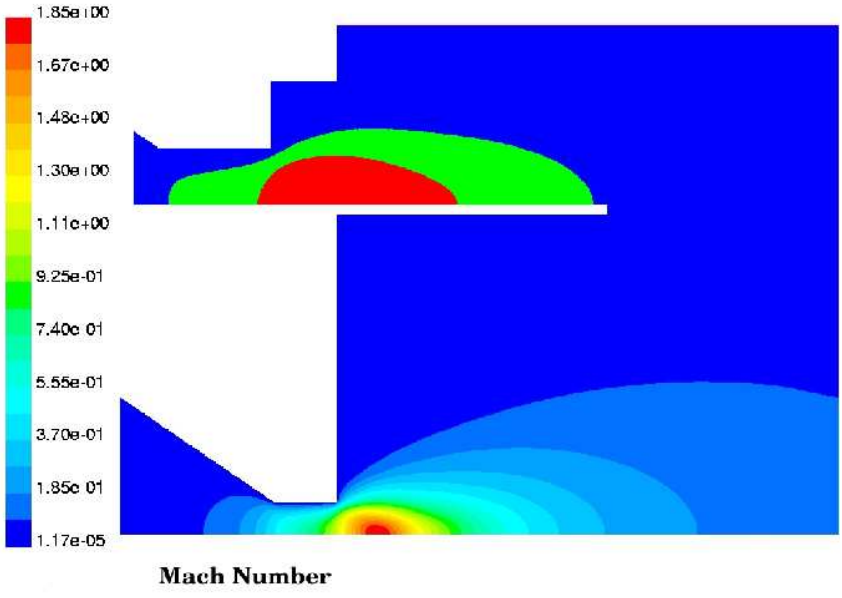

Figure 12: Flow field in backward micro-nozzle with a diameter of $D = 25$ μm, $P_{out}/P_0 = 0.1$, Mach contours.